

ASYMMETRIC SUPERCARDIOID BEAMFORMING USING CIRCULAR MICROPHONE ARRAYS

Yaakov Buchris and Israel Cohen

Technion, Israel Institute of Technology
Technion City, Haifa 32000, Israel
{bucris@campus, icohen@ee}.technion.ac.il

Jacob Benesty

INRS-EMT, University of Quebec
800 de la Gauchetiere Ouest, Suite 6900
Montreal, QC H5A 1K6, Canada
benesty@emt.inrs.ca

ABSTRACT

We present a joint-diagonalization based approach for a closed-form solution of the asymmetric supercardioid, implemented with circular differential microphone arrays. These arrays are characterized as compact frequency-invariant superdirective beamformers, allowing perfect steering for all azimuthal directions. Experimental results show that the asymmetric supercardioid yields superior performance in terms of white noise gain, directivity factor, and front-to-back ratio, when additional directional attenuation constraints are imposed in order to suppress interfering signals.

Index Terms— Circular differential microphone arrays (CDMAs), asymmetric beampatterns, supercardioid.

1. INTRODUCTION

In some applications involving broadband speech signals, circular differential microphone arrays (CDMAs) [1, 2] are advantageous due to several desired properties, such as frequency-invariant (FI) directivity pattern, small physical dimensions, superdirectivity [3,4], and perfect steering for all azimuthal directions. Circular geometry in general is beneficial for applications like 3D sound recording where signals may come from any direction [5–8].

Previous works on differential microphone arrays (DMAs), both for linear and circular geometries [9–13], have considered only the case of symmetric beampatterns, which is an inherent limitation of the linear geometry. Yet, in different array geometries like the circular one, asymmetric design may lead to a substantial performance improvement.

Recently we have proposed an analytical model for asymmetric CDMAs which generalizes the traditional symmetric model [14, 15]. It is shown that an asymmetric model, compared to a symmetric one, achieves higher performances in terms of white noise gain (WNG), directivity factor (DF),

and front-to-back-ratio (FBR) due to a more flexible design under the constraints of the null directions. Herein, we propose an alternative approach to that in [14, 15], which yields a closed-form solution for the asymmetric FBR-optimal supercardioid directivity pattern, based on the joint-diagonalization approach. The proposed approach is computationally advantageous as it involves the inversion of a small-size matrix while the former solution requires calculation of a null-space matrix and maximization of a Rayleigh-quotient term. In the simulations section, we present a second-order asymmetric supercardioid design and demonstrate its benefits with respect to the symmetric design.

2. SIGNAL MODEL

Consider an acoustic source signal, $X(\omega)$, with $\omega = 2\pi f$ denoting the angular frequency, that propagates in an anechoic acoustic environment at the speed of sound, i.e., $c \approx 340$ m/s, and impinges on a uniform circular array (UCA) of radius r , consisting of M omnidirectional microphones, where the distance between two successive sensors is equal to

$$\delta = 2r \sin\left(\frac{\pi}{M}\right) \approx \frac{2\pi r}{M}. \quad (1)$$

The direction of $X(\omega)$ to the array is denoted by the azimuth angle θ_s , measured anti-clockwise from the x axis, i.e., at $\theta = 0^\circ$.

Assuming the far-field propagation, the time delay between the m th microphone and the center of the array is $\tau_m(\theta_s) = \frac{r}{c} \cos(\theta_s - \psi_m)$, $m = 1, 2, \dots, M$, where $\psi_m = \frac{2\pi(m-1)}{M}$ is the angular position of the m th array element. The m th microphone signal is

$$Y_m(\omega) = e^{j\varpi \cos(\theta_s - \psi_m)} X(\omega) + V_m(\omega), \quad m = 1, 2, \dots, M, \quad (2)$$

where $\varpi = \frac{\omega r}{c}$, $j = \sqrt{-1}$, and $V_m(\omega)$ is the additive noise at the m th microphone. In a vector form, (2) becomes

$$\mathbf{y}(\omega) = [Y_1(\omega) \cdots Y_M(\omega)]^T = \mathbf{d}(\omega, \theta_s) X(\omega) + \mathbf{v}(\omega), \quad (3)$$

This research was supported by the Israel Science Foundation (grant no. 576/16), the ISF-NSFC joint research program (grant No. 2514/17), and MAFAT-Israel Ministry of Defense.

where $\mathbf{d}(\omega, \theta_s)$ is the steering vector at $\theta = \theta_s$, i.e.,

$$\mathbf{d}(\omega, \theta_s) = \left[e^{j\varpi \cos(\theta_s - \psi_1)} \dots e^{j\varpi \cos(\theta_s - \psi_M)} \right]^T, \quad (4)$$

the superscript T is the transpose operator, the vector $\mathbf{v}(\omega)$ is defined similarly to $\mathbf{y}(\omega)$, and the acoustic wavelength is $\lambda = c/f$. It is assumed that $\delta \ll \lambda$, in order to approximate the differential of the pressure signal.

Assuming a 2D scenario, the FI beampattern of an N th-order DMA is given, for any steering angle θ_s , as [9, 16]

$$\mathcal{B}_N(\theta - \theta_s) = \sum_{n=0}^N a_{N,n} \cos^n(\theta - \theta_s), \quad (5)$$

where θ is the azimuth, and $\{a_{N,n}\}_{n=0}^N$ are real coefficients.

In order to design a practical beamformer, the vector $\mathbf{y}(\omega)$ should be multiplied by a complex vector, $\mathbf{h}(\omega)$, where $\mathbf{h}(\omega) = [H_1(\omega) H_2(\omega) \dots H_M(\omega)]^T$. The corresponding designed beampattern is

$$\mathcal{B}[\mathbf{h}(\omega), \theta] = \mathbf{h}^H(\omega) \mathbf{d}(\omega, \theta). \quad (6)$$

The vector $\mathbf{h}(\omega)$ can be obtained using the approaches presented in [14, 15], which are aimed to design $\mathcal{B}[\mathbf{h}(\omega), \theta]$ as close as possible to $\mathcal{B}_N(\theta - \theta_s)$ (in the mean-square error sense).

3. ASYMMETRIC BEAMPATTERN FOR CDMA S

Traditional designs of DMAs focus mainly on linear geometry which inherently dictates a symmetric beampattern. Accordingly, (5) is sufficient for FI beampatterns associated with DMAs. Recently, we extended that design to include also asymmetric beampatterns. Specifically, an N th-order asymmetric CDMA beampattern with the mainlobe steered to θ_s is [14, 15]

$$\begin{aligned} \mathcal{B}_N(\theta - \theta_s) &= \sum_{n=0}^N \xi_n \cos^n(\theta - \theta_s) + \sum_{n=0}^{\lfloor \frac{N-1}{2} \rfloor} \mu_n \sin^{2n+1}(\theta - \theta_s) \\ &+ \sum_{n=1}^{\lfloor \frac{N}{2} \rfloor} \zeta_n \cos(\theta - \theta_s) \sin^{2n-1}(\theta - \theta_s), \end{aligned} \quad (7)$$

which is a trigonometric polynomial of power N with $2N$ roots, and $\{\xi_0, \dots, \xi_N, \mu_0, \dots, \zeta_1, \dots\}$ are real coefficients. In fact, (7) can be equivalently expressed as

$$\mathcal{B}_N(\theta - \theta_s) = \sum_{n=0}^N a_n \cos[n(\theta - \theta_s)] + \sum_{n=1}^N b_n \sin[n(\theta - \theta_s)]. \quad (8)$$

In the following derivations, we use for convenience (8) instead of (7).

4. OPTIMAL ASYMMETRIC SUPERCARDIOID

The common directivity patterns in the context of microphone arrays are dipole, cardioid, hypercardioid, and supercardioid. These patterns, originally developed for linear geometry, are traditionally symmetric with respect to the steering angle, θ_s . In this section, we develop an asymmetric version of the supercardioid for CDMA S based on a joint-diagonalization approach. The supercardioid pattern maximizes the FBR [9], which is defined for a cylindrical noise field as

$$\mathcal{F} = \frac{\int_{-\pi/2}^{\pi/2} \mathcal{B}_N^2(\theta) d\theta}{\int_{\pi/2}^{3\pi/2} \mathcal{B}_N^2(\theta) d\theta}, \quad (9)$$

where we assume, without loss of generality, that the steering angle is $\theta_s = 0^\circ$. Let us define the following vector

$$\mathbf{q}(\theta) = [1, \cos(\theta), \dots, \cos(N\theta), \sin(\theta), \dots, \sin(N\theta)]^T. \quad (10)$$

Then, we can write that $\int_{-\pi/2}^{\pi/2} \mathcal{B}_N^2(\theta) d\theta = \mathbf{c}^T \mathbf{\Gamma}_f \mathbf{c}$ and $\int_{\pi/2}^{3\pi/2} \mathcal{B}_N^2(\theta) d\theta = \mathbf{c}^T \mathbf{\Gamma}_b \mathbf{c}$, where

$$\mathbf{c} = [a_0, a_1, \dots, a_N, b_1, \dots, b_N]^T \quad (11)$$

is a vector of length $2N + 1$ containing the coefficients of the asymmetric beampattern (8). The matrices $\mathbf{\Gamma}_f$ and $\mathbf{\Gamma}_b$ of size $(2N + 1) \times (2N + 1)$ are given by

$$\begin{aligned} [\mathbf{\Gamma}_f]_{l,k} &= \int_{-\pi/2}^{\pi/2} q_l(\theta) q_k(\theta) d\theta \quad l, k = 0, 1, \dots, 2N \\ [\mathbf{\Gamma}_b]_{l,k} &= \int_{\pi/2}^{3\pi/2} q_l(\theta) q_k(\theta) d\theta \quad l, k = 0, 1, \dots, 2N, \end{aligned} \quad (12)$$

where $q_i(\theta) \triangleq [\mathbf{q}(\theta)]_i$ is the i th element of the vector $\mathbf{q}(\theta)$.

It can be shown that $[\mathbf{\Gamma}_f]_{l,k} = 0$ and $[\mathbf{\Gamma}_b]_{l,k} = 0$ for $0 \leq l \leq N$ and $N + 1 \leq k \leq 2N$. Also, $[\mathbf{\Gamma}_f]_{l,k} = 0$ and $[\mathbf{\Gamma}_b]_{l,k} = 0$ for $N + 1 \leq l \leq 2N$ and $0 \leq k \leq N$. Therefore, the coefficients $\{a_n\}_{n=0}^N$ and $\{b_n\}_{n=1}^N$ are independent. Hence, the circular geometry provides more degrees of freedom in the design of optimal patterns such as the supercardioid, and additional directional constraints should be imposed. The first one is the distortionless constraint:

$$\mathcal{B}_N(\theta_s = 0^\circ) = 1, \quad (13)$$

leading to $\sum_{n=0}^N a_n = 1$. We can add up to $L \leq 2N$ attenuation constraints of the form:

$$\mathcal{B}_N(\theta = \theta_l) = g_l, \quad l = 1, 2, \dots, L, \quad (14)$$

where $0 \leq g_l \leq 1$. We formulate these constraints as

$$\mathbf{H}_c \mathbf{c} = \mathbf{g}, \quad (15)$$

where \mathbf{H}_c is the constraint matrix of size $(L+1) \times (2N+1)$, typically non-diagonal. Vector \mathbf{g} of length $L+1$ contains the coefficients g_l , $l = 1, 2, \dots, L$, and a single unity entry, satisfying (13).

Now we can formulate the optimization problem which provides the asymmetric supercardioid beampattern:

$$\max_{\mathbf{c}} \frac{\mathbf{c}^T \mathbf{\Gamma}_f \mathbf{c}}{\mathbf{c}^T \mathbf{\Gamma}_b \mathbf{c}} \quad \text{subject to } \mathbf{H}_c \mathbf{c} = \mathbf{g}. \quad (16)$$

In order to solve (16), both $\mathbf{\Gamma}_f$ and $\mathbf{\Gamma}_b$ can be jointly diagonalized as follows [17]:

$$\mathbf{T}^T \mathbf{\Gamma}_f \mathbf{T} = \mathbf{\Lambda}, \quad (17)$$

$$\mathbf{T}^T \mathbf{\Gamma}_b \mathbf{T} = \mathbf{I}_{2N+1}, \quad (18)$$

where

$$\mathbf{T} = [\mathbf{t}_1 \ \mathbf{t}_2 \ \cdots \ \mathbf{t}_{2N+1}] \quad (19)$$

is a full-rank square matrix of size $(2N+1) \times (2N+1)$, \mathbf{I}_{2N+1} is the identity matrix of size $(2N+1) \times (2N+1)$, and

$$\mathbf{\Lambda} = \text{diag}(\lambda_1, \lambda_2, \dots, \lambda_{2N+1}) \quad (20)$$

is a diagonal matrix of size $(2N+1) \times (2N+1)$ containing the eigenvalues of the matrix $\mathbf{\Gamma}_b^{-1} \mathbf{\Gamma}_f$ in a descending order, i.e., $\lambda_1 \geq \lambda_2 \geq \lambda_3 \geq \cdots \geq \lambda_{2N+1} \geq 0$. The columns of the matrix \mathbf{T} are

$$\mathbf{t}_l = \frac{\mathbf{t}'_l}{\sqrt{\mathbf{t}'_l{}^T \mathbf{\Gamma}_b \mathbf{t}'_l}}, \quad l = 1, 2, \dots, 2N+1, \quad (21)$$

where \mathbf{t}'_l is the l th eigenvector of the matrix $\mathbf{\Gamma}_b^{-1} \mathbf{\Gamma}_f$, corresponding to the l th eigenvalue λ_l . We also define the vector:

$$\mathbf{c}' = \mathbf{T}^{-1} \mathbf{c}. \quad (22)$$

Substituting (17), (18) and (22) to (16), we get the equivalent optimization problem:

$$\max_{\mathbf{c}'} \frac{\mathbf{c}'^T \mathbf{\Lambda} \mathbf{c}'}{\mathbf{c}'^T \mathbf{c}'} \quad \text{subject to } \mathbf{H}_c \mathbf{T} \mathbf{c}' = \mathbf{g}. \quad (23)$$

The solution to the unconstrained version of (23) is known to be $\lambda_{\max} = \lambda_1$, and for that case $\mathbf{c}'_{\text{opt}} = [\gamma, 0, 0, \dots, 0]$ where γ is a constant. Since we have $L+1$ constraints that should be satisfied, the optimal vector \mathbf{c}'_{opt} is of the form:

$$\mathbf{c}'_{\text{opt}} = [\gamma^T \mathbf{0}_{2N-L}^T]^T, \quad (24)$$

where γ is a vector of length $L+1$ and $\mathbf{0}_{2N-L}$ is a column vector containing $2N-L$ zeros. Taking a vector \mathbf{c}'_{opt} with more than $L+1$ non-zero elements may lead to inferior results as proven in [16] (See Property 2.3.1, pp.45). Therefore, (23) can be reduced to

$$\mathbf{H}_c \tilde{\mathbf{T}} \boldsymbol{\gamma} = \mathbf{g}, \quad (25)$$

where

$$\tilde{\mathbf{T}} = [\mathbf{t}_1 \ \mathbf{t}_2 \ \cdots \ \mathbf{t}_{L+1}] \quad (26)$$

is a matrix of size $(2N+1) \times (L+1)$ that contains the $L+1$ eigenvectors corresponding to the $L+1$ largest eigenvalues of the matrix $\mathbf{\Gamma}_b^{-1} \mathbf{\Gamma}_f$. The solution to (25) is

$$\boldsymbol{\gamma} = \left(\mathbf{H}_c \tilde{\mathbf{T}} \right)^{-1} \mathbf{g}. \quad (27)$$

Substituting (22) and (24) into (27), we have

$$\mathbf{c}_{\text{opt}} = \tilde{\mathbf{T}} \left(\mathbf{H}_c \tilde{\mathbf{T}} \right)^{-1} \mathbf{g}. \quad (28)$$

5. A DESIGN EXAMPLE

In this section, we present a design example of the second-order asymmetric supercardioid. Second-order designs require at least $M = 5$ microphones. Let us assume that the steering angle is $\theta_s = 0^\circ$ and we would like to impose two nulls at $\theta_1 = 90^\circ$ and $\theta_2 = 245^\circ$. We choose $r = 0.75$ cm which leads to $\delta = 0.88$ cm.

First, we need to find the corresponding analytical asymmetric beampattern. Solving (28), the optimal coefficients vector, \mathbf{c} (11), is calculated and substituted into (8). The two additional roots are $\theta_3 = 133^\circ$, and $\theta_4 = 190^\circ$. Figure 1(a) shows the analytical beampattern of the second-order asymmetric design (blue solid line), its symmetric version (black dashed line), i.e., the beampattern for the case that $\theta_3 = 115^\circ$, and $\theta_4 = 270^\circ$, and also the second-order unconstrained symmetric supercardioid (red circles line), which was derived in [9] and obtained for nulls at $\theta_1 = 106^\circ$, and $\theta_2 = 153^\circ$. The latter is obtained by a direct optimization of the FBR without any constraints on the null directions. Figure 1(b) shows a second example where two directional constraints $\theta_1 = 115^\circ$ and $\theta_2 = 230^\circ$ were imposed. Table 1 summarizes the FBR values obtained by the three compared approaches for both examples. One can see that compared to the symmetric approach, the asymmetric design is significantly less sensitive than the symmetric design to the values of θ_1 and θ_2 . Furthermore, the asymmetric design achieves higher FBR values, which are closer to those values obtained by the unconstrained approach.

Table 1: Front-to-Back-Ratio, \mathcal{F} [dB], Achieved by Each of the Designs of a Second-Order Supercardioid for Two Different Choices of Constraints.

	$\theta_1 = 90^\circ$ $\theta_2 = 245^\circ$	$\theta_1 = 115^\circ$ $\theta_2 = 230^\circ$
Asymmetric	22.97	24.23
Symmetric	9.44	22.30
Unconstrained symmetric	26.31	26.31

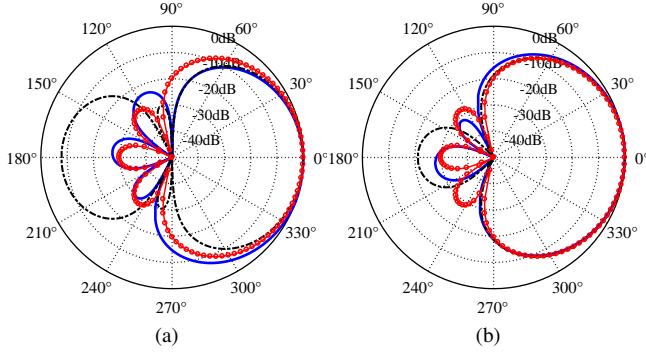


Fig. 1: Beampatterns for the second-order asymmetric supercardioid (blue solid line) and its symmetric version (black dashed line). The red circles line is the unconstrained second-order symmetric supercardioid [9]. (a) $\theta_1 = 90^\circ$, $\theta_2 = 245^\circ$. (b) $\theta_1 = 115^\circ$, $\theta_2 = 230^\circ$.

Using the calculated values of c (11) and of $\{\theta_i\}_{i=1}^4$, we can calculate $\mathbf{h}(\omega)$ using one of the methods presented in our previous work [14, 15] and design the second-order asymmetric supercardioid. In the following, we consider only the first example, i.e., the one with the parameters $\theta_1 = 90^\circ$ and $\theta_2 = 245^\circ$.

Figure 2 shows the WNG, the DF, and the FBR¹ as a function of frequency for the second-order asymmetric supercardioid (blue solid line), the second-order symmetric supercardioid (black dashed line), and the second-order unconstrained symmetric supercardioid (red circles line). These performance measures are defined as [16]

$$\mathcal{W}[\mathbf{h}(\omega)] = \frac{|\mathbf{h}^H(\omega) \mathbf{d}(\omega, \theta_s)|^2}{\mathbf{h}^H(\omega) \mathbf{h}(\omega)}, \quad (29)$$

$$\mathcal{D}[\mathbf{h}(\omega)] = \frac{|\mathbf{h}^H(\omega) \mathbf{d}(\omega, \theta_s)|^2}{\mathbf{h}^H(\omega) \mathbf{\Gamma}_{\text{dn}}(\omega) \mathbf{h}(\omega)}, \quad (30)$$

$$\mathcal{F}[\mathbf{h}(\omega)] = \frac{\int_{-\pi/2}^{\pi/2} \mathcal{B}^2[\mathbf{h}(\omega), \theta] d\theta}{\int_{\pi/2}^{3\pi/2} \mathcal{B}^2[\mathbf{h}(\omega), \theta] d\theta}, \quad (31)$$

where

$$[\mathbf{\Gamma}_{\text{dn}}(\omega)]_{ij} = \text{sinc}\left(\frac{2\omega r}{c} \left| \sin\left[\frac{\pi(i-j)}{M}\right] \right|\right). \quad (32)$$

The performance of the asymmetric design is very similar to that of the unconstrained supercardioid in terms of WNG, DF, and FBR while the symmetric design achieves much lower FBR and similar DF. In [14], we derive also the asymmetric hypercardioid and show that the asymmetric

¹for a cylindrical noise field

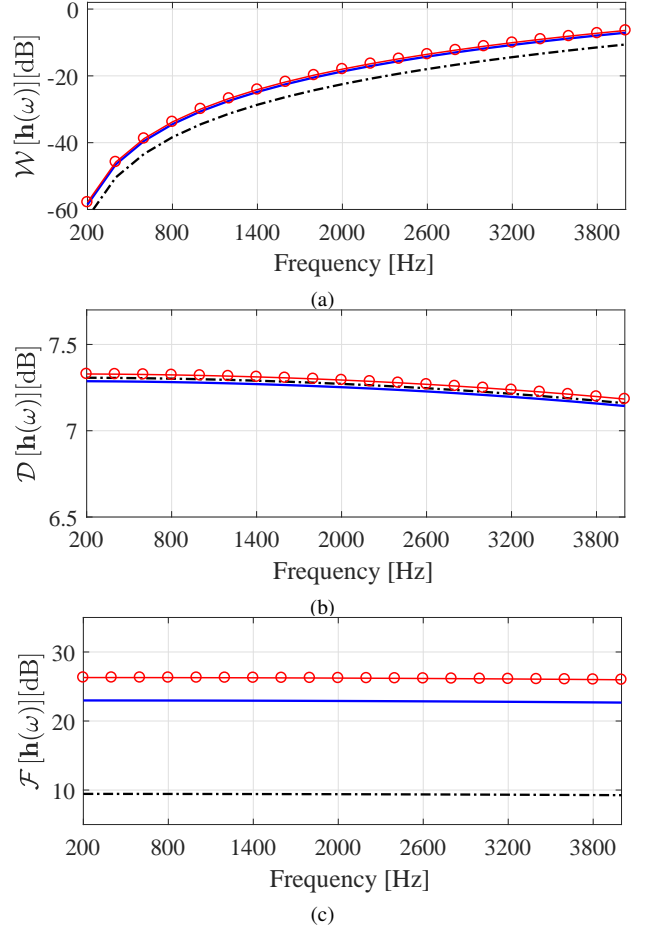


Fig. 2: WNG (a), DF (b), and FBR (c) vs. frequency for the second-order asymmetric supercardioid (blue solid line), the second-order symmetric design (black dashed line), and the second-order unconstrained symmetric supercardioid (red circles line) with $M = 5$ sensors. $\theta_1 = 90^\circ$, $\theta_2 = 245^\circ$.

design can achieve superior performance also in terms of DF. In addition, practical methods to improved the WNG, based either on regularization methods or increasing the number of sensors, can be found in [18] and are not included here as we would like to concentrate on the comparison between symmetric and asymmetric designs.

6. CONCLUSIONS

We have presented an alternative solution to an asymmetric supercardioid, which is based on the joint-diagonalization approach. The proposed solution is computationally more efficient than an existing alternative solution. Simulation results demonstrate that the asymmetric model yields a more flexible design and superior performance in several real-world applications involving beamforming for speech signals such as teleconferencing, hand-free communications, and more.

7. REFERENCES

- [1] J. Benesty, J. Chen, and I. Cohen, *Design of Circular Differential Microphone Arrays*. Berlin, Germany: Springer-Verlag, 2015.
- [2] Y. Buchris, I. Cohen, and J. Benesty, "Analysis and design of time-domain first-order circular differential microphone arrays," in *the 22nd International Congress on Acoustics (ICA)*, 2016.
- [3] H. Cox, R. M. Zeskind, and T. Kooij, "Practical supergain," *IEEE Trans. Acoust., Speech, Signal Processing*, vol. ASSP-34, no. 3, pp. 393–397, June 1986.
- [4] M. Crocco and A. Trucco, "Design of robust superdirective arrays with a tunable tradeoff between directivity and frequency-invariance," *IEEE Trans. Signal Process.*, vol. 59, no. 5, pp. 2169–2181, May 2011.
- [5] H. Teutsch and W. Kellerman, "Acoustic source detection and localization based on wavefield decomposition using circular microphone arrays," *J. Acoust. Soc. Amer.*, vol. 120, no. 5, pp. 2724–2736, Nov. 2006.
- [6] P. Ioannides and C. A. Balanis, "Uniform circular and rectangular arrays for adaptive beamforming applications," *IEEE Antennas Wireless Propagat. Lett.*, vol. 4, pp. 351–354, 2005.
- [7] Y. L. Ma, Y. Yang, Z. He, K. Yang, C. Sun, and Y. Wang, "Theoretical and practical solutions for high-order superdirectivity of circular sensor arrays," *IEEE Trans. Ind. Electron.*, vol. 60, pp. 203–209, 2013.
- [8] H. H. Chen, S. C. Chan, and K. L. Ho, "Adaptive beamforming using frequency invariant uniform concentric circular arrays," *IEEE Trans. Circuits Syst. I, Reg. Papers*, vol. 54, no. 9, pp. 1938–1949, Sept. 2007.
- [9] G. W. Elko, "Superdirectional microphone arrays," in *Acoustic Signal Processing for Telecommunication*, S. L. Gay and J. Benesty, Eds. Boston, MA: Kluwer Academic Publishers, 2000, ch. 10, pp. 181–237.
- [10] T. D. Abhayapala and A. Gupta, "Higher order differential-integral microphone arrays," *J. Acoust. Soc. Amer.*, vol. 127, pp. 227–233, May 2010.
- [11] J. Benesty and J. Chen, *Study and Design of Differential Microphone Arrays*. Berlin, Germany: Springer-Verlag, 2012.
- [12] E. De Sena, H. Hacıhabibğlu, and Z. Cavetković, "On the design and implementation of higher order differential microphones," *IEEE Trans. Audio, Speech, Language Process.*, vol. 20, no. 1, pp. 162–174, Jan. 2012.
- [13] Y. Buchris, I. Cohen, and J. Benesty, "First-order differential microphone arrays from a time-domain broadband perspective," in *International Workshop on Acoustic Echo and Noise Control (IWAENC) 2016 conf.*
- [14] —, "Frequency-domain design of asymmetric circular differential microphone arrays," *IEEE/ACM Transactions on Audio, Speech, and Language Processing*, 2018.
- [15] —, "Asymmetric beampatterns with circular differential microphone arrays," in *IEEE Workshop on Applications of Signal Processing to Audio and Acoustics (WASPAA)*, 2017.
- [16] J. Benesty, I. Cohen, and J. Chen, *Fundamentals of Signal Enhancement and Array Signal Processing*. Wiley-IEEE Press, 2017.
- [17] J. N. Franklin, *Matrix Theory*. Englewood Cliffs, NJ: Prentice-Hall, 1968.
- [18] J. Benesty, J. Chen, and C. Pan, *Fundamentals of Differential Beamforming*. Springer, 2016.